The FEBS Journal

FEBS PRESS science publishing by scientists

Brca2 abrogation engages with the alternative lengthening of telomeres via break-induced replication

Mi-Sun Kwon[1], Jennifer J. Lee[1], Jaewon Min[1], Kwangwoo Hwang[1], Seung Gu Park[2], Eun-Hye Kim[2], Byung Chul Kim[3], Jong Bhak[2,3] and Hyunsook Lee[1]

1 Department of Biological Sciences, Institute of Molecular Biology and Genetics (IMBG), Seoul National University, South Korea
2 Department of Biomedical Engineering, UNIST, Ulsan, Korea
3 Clinomics Inc., Ulsan, Korea

Keywords
ALT mouse; alternative lengthening of telomeres; Brca2; break-induced replication

Correspondence
H. Lee, Department of Biological Sciences, Institute of Molecular Biology and Genetics (IMBG), Seoul National University, 1 Gwanak-Ro, Gwanak-Gu, Seoul 08826, South Korea
Tel: +82 2 886 4339
E-mail: HL212@snu.ac.kr

(Received 17 August 2018, revised 21 January 2019, accepted 25 February 2019)

doi:10.1111/febs.14796

A subset of cancer cells maintains their telomeres without telomerase through the recombination-based alternative lengthening of telomeres (ALT) pathway. Currently, it is not yet clear in what context ALT is induced and how the pathway choice is made. Here, we show that abrogation of *Brca2* reinforces break-induced replication (BIR) and engages with ALT pathway. Brca2 depletion in telomerase-null mouse cells alleviated the growth defect, accompanied by telomere elongation, suggesting the induction of ALT. We also found that Brca2-depleted telomerase-null cells exhibited dynamic clustering of telomeres from G2 phase in Promyelocytic Nuclear (PML) bodies. For Brca2-deficient ALT induction, Rad51 was dispensable but Mre11 and Rad52 were required. Congruently, conservative telomeric DNA synthesis was apparent in mitosis, indicating that the absence of Brca2 directed towards Rad52-mediated BIR. Collectively, we propose that Brca2 abrogation can instigate ALT tumourigenesis through the induction of BIR. This study implies that inhibitors of BIR may be useful for BRCA2-associated ALT-type cancers. Assessing ALT features may be considered for the tailored therapy of BRCA2-associated cancers.

Introduction

The linearity of eukaryotic chromosomes poses many problems, including replication and the protection of chromosome ends against nucleolytic attacks. During neoplastic transformation, telomerase is reactivated to overcome the telomere replication problem, which allows cancer cells to replicate their DNA indefinitely avoiding telomere shortening. About 10% of cancer cells, however, do not express telomerase. Instead, they utilize recombination to elongate telomeres, and these are classified as alternative lengthening of telomeres (ALT) cancers [1]. In yeast, cells that survive out from the deficiency of telomerase activity had been grouped in two different types: Type I that requires Rad51 and type II that is devoid of Rad51 but requires Rad59, a homolog of Rad52 [2]. Homologous recombination that requires Rad51 had been suggested for some time for the underlying mechanism of ALT cancers [3]. More recently, break-induced replication (BIR) has been suggested to be responsible for ALT [4,5], indicating that type I and type II-like ALT pathways are also present in mammals. However, how ALT-type tumourigenesis begins and what determines the

Abbreviations
4-OHT, tamoxifen; ALT, alternative lengthening of telomeres; APBs, ALT-associated PML bodies; BIR, break-induced replication; CO-FISH, chromosome orientation-FISH; DSB, double-strand break; HDR, homology-directed repair; HR, homologous recombination; MiDAS, mitotic DNA synthesis; PML, promyelocytic leukaemia; Q-FISH, quantitative fluorescence *in* situ hybridization; SV40 LT, SV40 large T antigen; T-SCE, telomeric sister chromatid exchange.

different recombination pathways in ALT remains unknown.

Brca2 is a multifunctional tumour suppressor with crucial activities in maintaining genome and chromosome integrity throughout the cell cycle [6]. In S/G2 phase, Brca2 is critically required for error-free double-strand break (DSB) repair via homologous recombination (HR), also called homology-directed repair (HDR), because of its role in regulating Rad51 filament formation [7,8]. Independent from its role in HDR, Brca2 protects stalled replication forks from collapsing [9,10]. Consistently, Brca2 is also involved in telomere replication homeostasis: it inhibits MRE11-mediated resection of stalled replication forks at the telomeres [11] and/or loads Rad51 for efficient telomere replication and capping [12]. Therefore, the loss of Brca2 results in progressive shortening of telomeres and growth arrest [11,12].

As the shortening of telomeres triggered by Brca2 deficiency is not related to telomerase expression and is incompatible with the fact that dysfunctional Brca2 leads to tumourigenesis, we had asked whether the paradoxical occurrence of neoplastic transformation is due to the induction of ALT. We showed in *Caenorhabditis elegans* that depletion of BRC-2, an orthologue of Brca2, results in a delay of senescence, accompanied by telomere length elongation [13]. Similarly, abrogation of *Brh2*, an orthologue of *Brca2* in fungus, *Ustilago maydis*, led to an ALT-like feature [14]. Here, we asked whether this function of *Brca2* in suppressing ALT is conserved in mice. Moreover, we wanted to see whether one could monitor the process of ALT induction using mouse models, simultaneously revealing the molecular mechanism beneath ALT induction. Finally, we asked if Brca2 lies in the crossroad of decision-making among different recombination mechanisms.

Results

Induction of ALT after *Brca2* abrogation in telomerase-deficient mice

To ask if ALT can be induced after depleting Brca2 in mice, we first developed a mouse model in telomerase-deficient background. Conditional *Brca2* knockout mice were crossed to telomerase-null mice, so that Brca2 abrogation be controlled in time and space. This mouse model was generated via several intercrosses of telomerase RNA-deficient $mTR^{+/-}$ mice [15,16], tamoxifen-inducible $Cre\text{-}ER^{TM}$ mice [17] and finally $Brca2^{F11/F11}$ mice [18]. As mice have long telomeres, the effects of telomere shortening and subsequent ALT induction can only be observed after several generations of telomerase-deficient mice breeding [15]. We faced difficulties in observing the development of spontaneous ALT-type cancers in *Brca2*-deficient and telomerase-deficient (double-null) mice, due to tedious breeding up to sixth generation [15] and the inefficiency of *Brca2* depletion post tamoxifen feeding. To overcome these problems, we developed an *ex vivo* model of ALT induction by utilizing the organoid culture of the pancreas.

Organoids are a three-dimensional culture of the epithelial stem cells [19] that can mimic the way the cells grow and differentiate into organs. As organoids are regarded *ex vivo* organs [20], one could monitor the process of organ growth and the initiation of tumourigenesis. Long-term culture of the organoids might overcome the time-consuming breeding of telomerase-deficient mice and recapitulate the physiology of continued cell proliferation and precipitate telomere problems. That inherited mutations of *Brca2* predisposes to pancreas cancers [21] was also considered in choosing pancreas organoid system.

Pancreas ductal epithelial cells were isolated from third generation (G3) mice of $Terc^{-/-}$ ($mTR^{-/-}$) that were crossed to $Brca2^{F11/F11}$, $Cre\text{-}ER^{TM}$, and subjected to three-dimensional culture as reported [20]. Thirteen days after the first organoids grew out, organoids were mechanically dissociated and passed through the sieve to collect similar sizes. A hundred organoids of ~ 100 μm were plated in duplicates: one set was treated with tamoxifen (4-OHT) to create $Brca2^{F11}$ allele, and the other left alone for control (Fig. 1A Top and B, [I]). The growth of the organoids was assessed by size and numbers at day 12 and replated in 1 : 6 ratio to assess whether Brca2 depletion in telomerase-null background can rescue senescence (Fig. 1A bottom and C, [II] & [III]).

RNA component of telomerase deficiency ($mTR^{-/-}$) alone at first did not interfere with the growth of the organoids (Fig. 1C, [I]). However, in the prolonged culture, telomerase deficiency led to growth defect (Fig. 1C, II & III, −4-OHT). In comparison, *Brca2* deletion resulted in precipitated growth retardation in organoids (Fig. 1B, +4-OHT), as was in the animal [22–24]. In telomerase-negative background ($mTR^{-/-}$), *Brca2* depletion led to a growth defect in the initial phase (Fig. 1C, [I], +4-OHT). In comparison, the depletion of *Brca2* allele overcame the growth defect of $mTR^{-/-}$ organoids in long-term culture (Fig. 1C, II and III, +4-OHT). The result from the mouse pancreas organoid culture recapitulated the phenomena observed from telomerase mutant worms [13], suggesting that depletion of *Brca2* in inducing ALT is evolutionarily conserved.

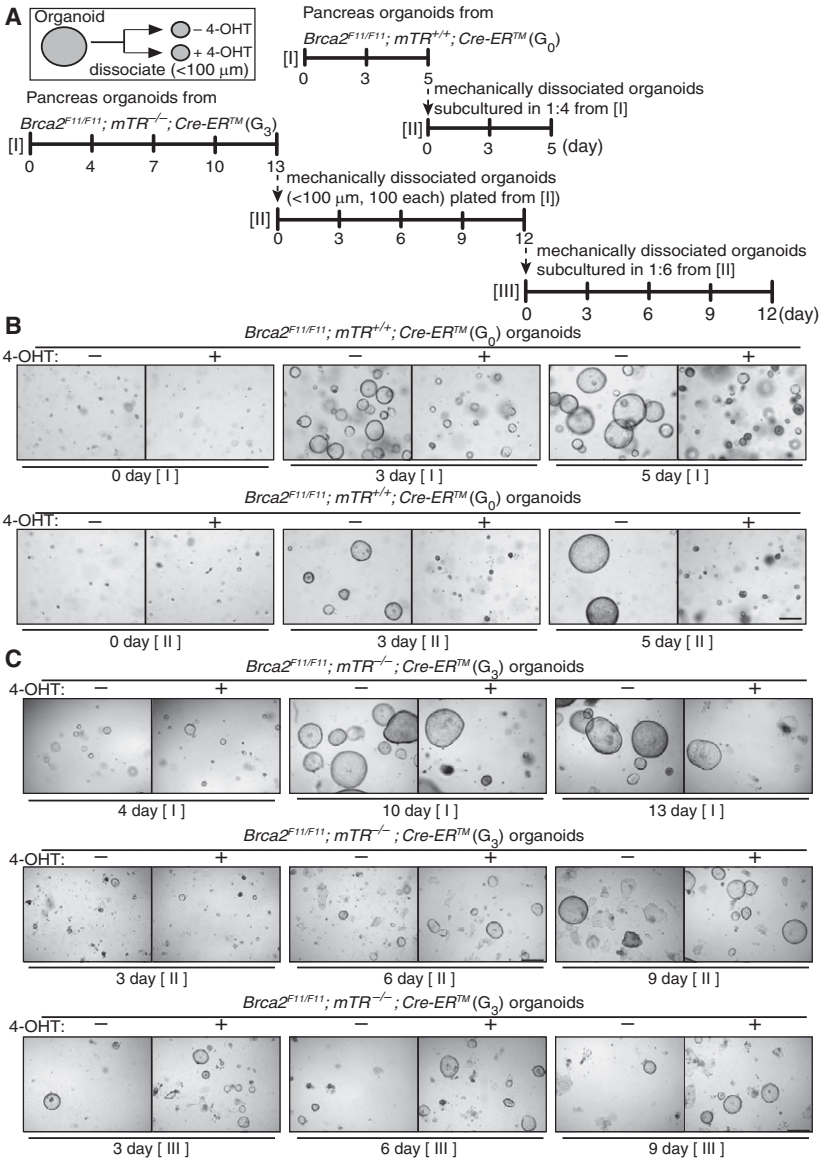

Fig. 1. Abrogation of Brca2 gradually overcomes the growth defect of the telomerase-null organoids. (A) Top; A schematic diagram of the assay for (B) that showed how mouse pancreas organoid cultures of *Brca2*$^{F11/F11}$; *mTR*$^{+/+}$; *Cre-ER*^{TM} were compared for their growth with (−4-OHT) or without (+4-OHT) *Brca2*. Bottom; A schematic diagram of the assay for C. It shows the way how mouse pancreas organoid cultures of third generation *Brca2*$^{F11/F11}$; *mTR*$^{-/-}$; *Cre-ER*^{TM} (G3) were passaged to compare growth with (−4-OHT) or without (+4-OHT) Brca2. (B) *Brca2*$^{F11/F11}$ and *Cre-ER*^{TM} mice were bred to create telomerase-positive *mTR*$^{+/+}$ mice. Ductal epithelial cells were isolated, same number of cells were seeded in duplicate and subjected to three-dimensional organoid cultures. Treatment of tamoxifen (4-OHT) induces the creation of *Brca2*^{F11} allele. Organoids from phase [I] were dissociated mechanically and passed through the sieve to collect organoids smaller than 100 μm. Representative images of Phase [I–II] at days with (+) or without (−) 4-OHT. (C) Telomerase-deficient mice (*Terc*-null; *mTR*$^{-/-}$) were bred for three generations with *Brca2*$^{F11/F11}$ and *Cre-ER*^{TM} (G3). Organoids from phase [I] were dissociated mechanically and passed through the sieve to collect organoids smaller than 100 μm. A hundred organoids were seeded on day 0 of phase [II]. From day 12 of [II], all organoids were mechanically dissociated and diluted 1 : 6 ratio, then seeded (day 0, phase [III]). Representative images of Phase [I–III] at days with (+) or without (−) 4-OHT.

To assess the effects on telomere length post-*Brca2* deletion in telomerase knockout mice, MEFs from first to fourth generation were isolated, infected with or without *Ad-Cre* and subjected to quantitative fluorescence *in situ* hybridization (Q-FISH) [25] to measure telomere length (Fig. 2A, left and Bottom). Progressive

shortening of telomeres was observed in telomerase-deficient MEFs ($mTR^{-/-}$; $Brca2^{F11/F11}$; $-Ad\text{-}Cre$). Brca2-deficiency in this setting exacerbated the telomere shortening in an early generation ($mTR^{-/-}$; $Brca2^{F11/F11}$; $+Ad\text{-}Cre$, G1 & G2). However, Brca2 deletion alleviated further telomere shortening in a later generation of telomerase knockout mice ($mTR^{-/-}$; $Brca2^{F11/F11}$; $+Ad\text{-}Cre$, G4).

Although Brca2 depletion overcame the senescence of telomerase-deficient MEFs, collecting enough numbers of cells to analyse telomeres was not feasible due to poor growth. To overcome the problem, later generation (G4) MEFs of $Brca2^{F11/F11}$; $mTR^{-/-}$; $Cre\text{-}ER^{TM}$ were immortalized by transduction with a lentivirus encoding SV40 LT (Large T antigen). Then telomere lengths were compared in cells with or without tamoxifen (4-OHT) treatment. The result showed that Brca2 abrogation after tamoxifen treatment led to elongation of net telomere lengths, compared to telomerase-null alone (Fig. 2A, right). Furthermore, telomeric C-circles, one of the hallmarks of ALT [26], were markedly elevated in double-null MEFs depleted of p53, but not in wild-type or heterozygous for telomerase RNA ($mTR^{+/-}$), supporting that an ALT-like feature is indeed induced after the abrogation of Brca2 (Fig. 2B). Similar results were obtained without *p53* depletion, indicating that C-circle increase was not due to the absence of p53, but a result from Brca2 abrogation (Fig. 2C).

Telomeres exhibit dynamic clustering at the PML bodies in MEFs doubly null for Brca2 and telomerase

Studies from cancer cell lines showed that telomeres exhibit directional movement for synapsis in ALT [3]. We asked if a similar pattern could be detected after Brca2 depletion in telomerase knockout MEFs. TRF1 (TTAGGG repeat binding factor 1) that localizes to telomeres [27] was tagged with GFP, and the expression plasmid was transfected into MEFs to monitor telomere movements.

As Brca2 localizes to telomeres in S phase [11], we decided to monitor the telomere movement from S/G2 phase. MEFs were serum starved for 16 h and released for 2 h to enrich S phase cells before time-lapse live imaging (Fig. 3A). The effect of Brca2 depletion was assessed in third generation (G3) telomerase-null MEFs, because the result from Fig. 2 suggested that shortening and deprotection of telomeres precede telomeric recombination after Brca2 abrogation.

During time-lapse video microscopy, which started 2 h post serum stimulation and continued for ~ 18 h (Fig. 3A), dynamic association then disassociation of telomeres were detected when Brca2 was abolished from telomerase-null cells (Fig. 3B and Movie S2 and S3). The result suggests that clustering took place from and after G2 phase. The observed association was predominant between two telomeres, but often included more than two (Fig. 3B, enlarged insets and arrows, Movie S2 and S3). None of the WT ($Brca2^{F11/F11}$ −4-OHT, data not shown), Brca2-deficient ($Brca2^{F11/F11}$; $mTR^{+/+}$ +4-OHT, data not shown) or telomerase-null MEFs (Fig. 3B, −4-OHT, Movie S1) displayed clustering during 18 h of video microscopy.

Of note, TRF1 fluorescence intensity was low, compared to wild-type (data not shown), in G3 MEFs of telomerase-null MEFs (Movie S1, Fig. 2B, −4-OHT), confirming that without telomerase, telomeres shorten with generations. Then the fluorescence intensity of TRF1 increased in a heterogeneous manner in double-null MEFs (Fig. 3B, +4-OHT; Movie S2 and S3), indicating that telomeres shortened in G3 MEFs of telomerase-null, then were elongated upon depletion of Brca2.

The average clustering of telomeres in double-null MEFs was five events per cell (Fig. 3C). Nearly all of the double-null MEFs displayed more than two clustering events (Fig. 3D). Notably, micronuclei, the result of chromosome mis-segregation, were frequently

Fig. 2. Brca2 abrogation in telomerase-deficient MEFs elongates the net telomere lengths. (A) Telomere lengths measured by T-FISH in different generations (G1, G2, G4) with (+) or without (−) *Ad-Cre* infection (Left). Infection with *Ad-Cre* (+Cre) creates $Brca2^{F11}$ allele. *Y*-axis, telomere lengths are shown as arbitrary units of fluorescence intensity from T-FISH. Telomerase-positive ($mTR^{+/+}$) and heterozygous ($mTR^{+/-}$) mice that were bred and maintained for more than three generations were employed for control. (Right) Telomere length measured in immortalized MEFs of generation 4. $Brca2^{F11/F11}$; $mTR^{-/-}$; $Cre\text{-}ER^{TM}$ MEFs (G4) were transduced with lentivirus encoding SV40 LT for immortalization. Addition of 4-OHT deletes *Brca2* allele. Western blot analysis with a home-made antibody that detects mouse Brca2 [28] confirmed the deletion of Brca2 (WT) and the creation of $Brca2^{F11}$ allele after infection with *Ad-Cre* in telomerase-positive ($mTR^{+/+}$), first generation and 4th generation of telomerase-null ($mTR^{-/-}$) MEFs. $Brca2^{F11}$ allele is an in-frame deletion of exon 11, creating truncated protein [11,28]. (B) Signs of ALT induction. C-circle (CC) assay [26] in indicated mouse genotypes after depletion of p53 with lentiviral infection of *shRNA* (*shTrp53*). MEFs were isolated from second-generation mice and treated with 4-hydroxytamoxifen (4-OHT) to generate $Brca2^{F11}$ allele. p53 was depleted to avoid the low viability of fibroblasts doubly null for telomerase and *Brca2*. (C) CC assay without interfering *p53*. MEFs were subjected to adenoviral infection (Ad-Cre) 3 days before genomic DNA extraction. Ad-GFP adenovirus was used as a control (−).

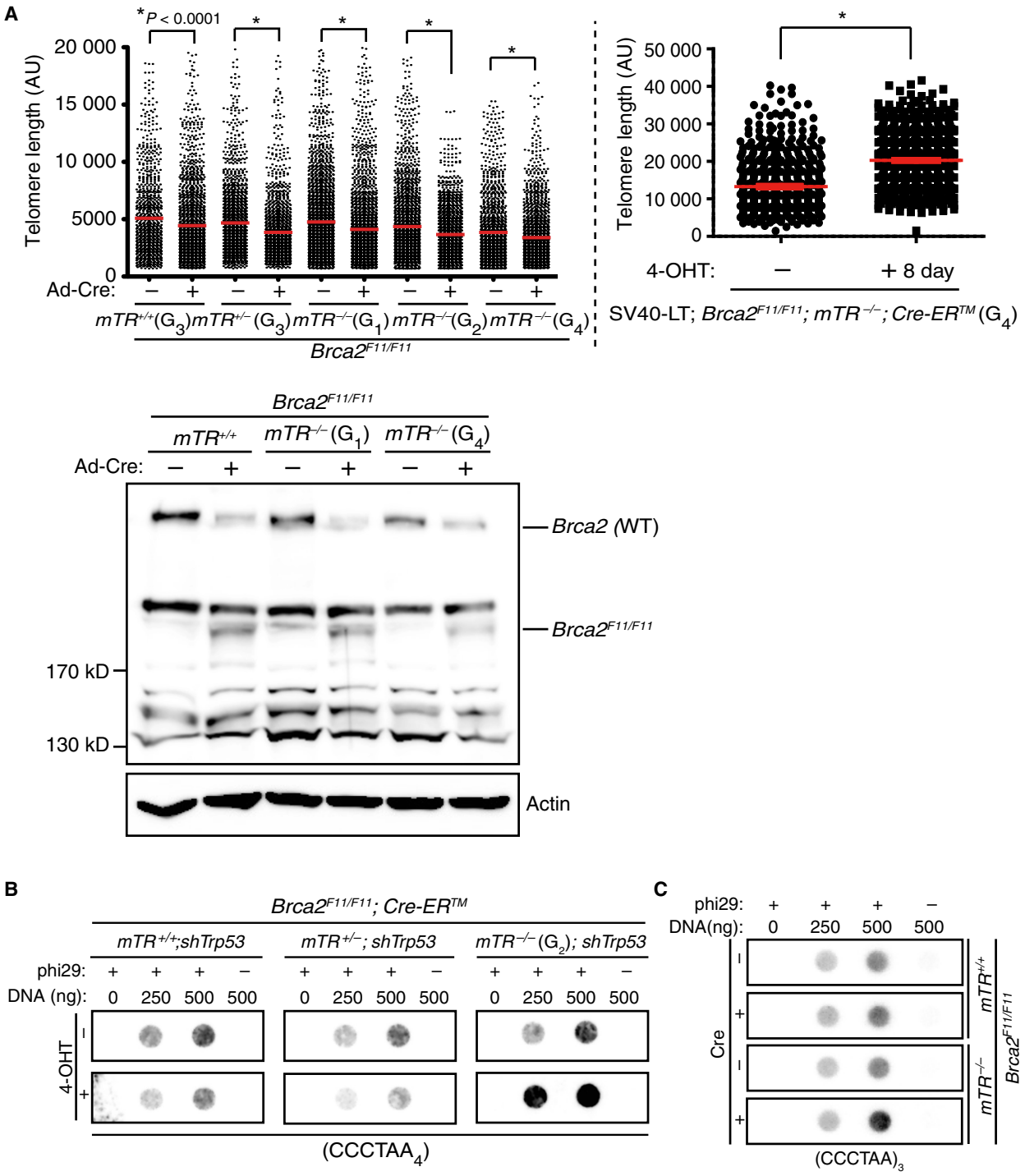

detected in Brca2-deficient MEFs (Fig. 3E), consistent with the role of Brca2 in mitosis [28]. Interestingly, the absence of telomerase with Brca2 markedly increased the incidence of micronuclei (Fig. 3E).

We then asked whether telomere clustering was associated with telomere-containing Promyelocytic Leukaemia (PML) bodies (APBs), as APBs are one of the hallmarks of ALT [29–32] and is thought to be the sites of telomere recombination [29,33]. A DsRed-tagged *PML4*-expressing construct was cotransfected with a *TRF1-EGFP*-expressing construct, and the cells were subjected to time-lapse video microscopy.

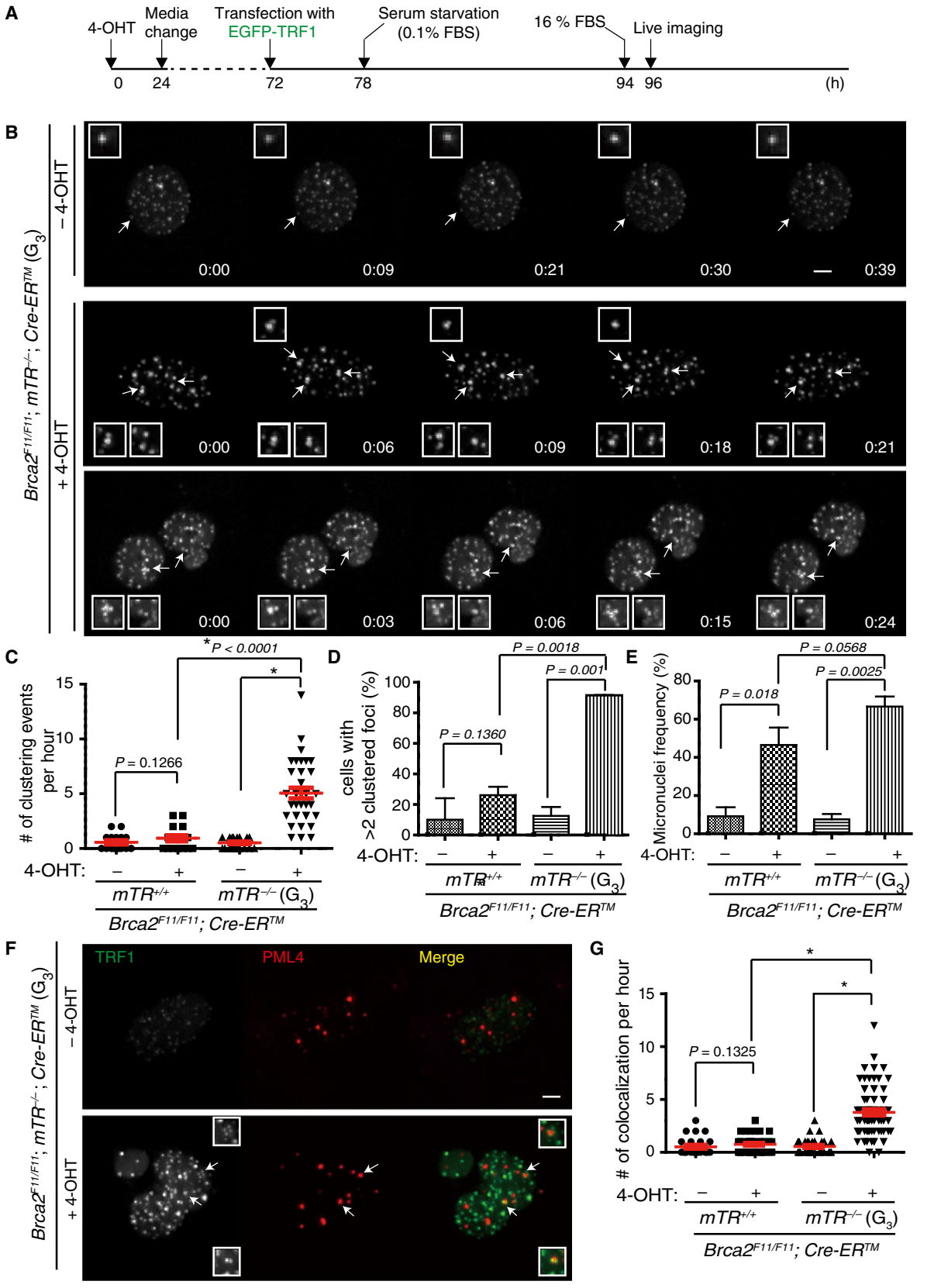
A
4-OHT
Media change
Transfection with EGFP-TRF1
Serum starvation (0.1% FBS)
16 % FBS
Live imaging
0
24
72
78
94
96
(h)
B
Brca2F11/F11; mTR−/−; Cre-ERTM (G3)
– 4-OHT
+ 4-OHT
0:00
0:09
0:21
0:30
0:39
0:06
0:18
0:03
0:15
0:24
C
# of clustering events per hour
P = 0.1266
*P < 0.0001
*
4-OHT:
mTR+/+
mTR−/− (G3)
Brca2F11/F11; Cre-ERTM
D
cells with >2 clustered foci (%)
P = 0.1360
P = 0.0018
P = 0.001
E
Micronuclei frequency (%)
P = 0.018
P = 0.0568
P = 0.0025
F
TRF1
PML4
Merge
G
# of colocalization per hour
P = 0.1325

Fig. 3. Clustering of telomeres at the PML body in cells doubly deficient in *Brca2* and telomerase. (A) Schematic drawing of the experiment. Tamoxifen (4-OHT) was treated to generate $Brca2^{F11/F11}$ allele when needed (data not shown), before transfection of *EGFP-TRF1*-expressing construct for live imaging of telomere movements. Cells were serum starved for 16 h then released for 2 h before imaging. (B) Representative time-lapse captured images of telomere movements in generation 3 (G3) of $Brca2^{F11/F11}$; $mTR^{-/-}$; $Cre\text{-}ER^{TM}$ with or without 4-OHT. Enlarged images of telomeres marked with arrows are shown in the square. Movies corresponding to the figures are provided as supplementary videos (Movie S1–S3). Scale bar, 10 μm. (C) All clustering events were scored and marked. Number of cells analysed: $Brca2^{F11F11}$ −4-OHT, $n = 16$; $Brca2^{F11F11}$ +4-OHT, $n = 16$; $Brca2^{F11F11}$; $mTR^{-/-}$ (G3) −4-OHT, $n = 21$; $Brca2^{F11F11}$; $mTR^{-/-}$ (G3) +4-OHT, $n = 35$. (D) Percentage of cells with more than two clustering telomeres. (E) The frequency of micronuclei with or without Brca2 and/or telomerase. (F) Association of clustering telomeres with PML bodies. *EGFP-TRF1*- and *DsRED-PML4*-expressing constructs were transfected, and telomere movements were monitored in time-lapse video microscopy in the presence (Movie S4, grey) or absence of Brca2 (Movie S6, grey). In G3 double-null MEFs, telomeric clustering was associated with PML (Movie S7). Enlarged images of telomeres marked with arrows are shown in the square. Scale bar, 10 μm. (G) The frequency of TRF1 colocalizing with PML4. All *P* values were obtained with the Student's *t*-test (mean ± SEM).

PML4 formed distinct foci in Brca2-depleted telomerase-deficient MEFs (G3), and the telomere clustering was associated with the PML body, as indicated by colocalization of TRF1 and PML4 (Fig. 3F, +4-OHT, Movie S6 and S7). In comparison, there was no detectable TRF1 and PML4 colocalization in telomerase-deficient MEFs with intact Brca2 (Fig. 3F, −4-OHT, Movie S4 and S5). The overall fluorescence signal of TRF1 in telomerase-null MEFs was markedly low (Fig. 3F, −4-OHT), compared to double-null MEFs (+4-OHT), consistent with the notion that telomeres shorten in G3 of telomerase-deficient MEFs. There were approximately five APBs that colocalized with telomere clustering per hour in double-null of G3 MEFs (Fig. 3G).

Mre11 and Rad52 are required for the induction of ALT after Brca2 abrogation

Telomerase-deficient MEFs exhibited moderate elevation of telomeric DNA damage with generations (Fig. 4A). Intriguingly, Brca2 abrogation exacerbated the telomere damage at fourth generation in telomerase-null background (Fig. 4A, G4). Previously, we showed that Brca2-depleted MEFs exhibit fragile telomeres due to the collapse of stalled replication forks [11]. It is possible that the elevated replication stress provoked by Brca2 depletion in telomerase-deficient background triggered a telomeric recombination pathway.

We asked whether the role of Brca2 in telomere replication homeostasis was associated with the choice of molecular pathway after Brca2 abrogation. Fragility in telomeres was significantly increased in the third generation (G3) telomerase knockout cells after Brca2 abrogation (Fig. 4B, +4-OHT). The telomere fragility after Brca2 depletion was compromised when Mre11, the nuclease suggested to resect stalled replication forks [9], was depleted with *shRNA* (Fig. 4B, +4-OHT + *shMre11*). Unlike Brca2 abrogation, telomere fragility was not immediately detected when Rad51 was depleted (Fig. 4B, *shRad51* and +4-OHT + *shRad51*).

Congruently, Brca2 abrogation led to the increase in APBs, which was significantly decreased after Mre11 depletion (Fig. 4C, +4-OHT; +4-OHT + *shMre11*). A similar effect was observed when the inhibitor of Mre11, Mirin [34], was treated (Fig. 4D, +4-OHT; +4-OHT + Mirin). Consistent with the result of telomere fragility, APB was not observed after depletion of Rad51 (Fig. 4C, *shRad51*) or the inhibition of it by RI-1 [35] (Fig. 4D, RI-1). These results indicate that Rad51 depletion had little effect in primary MEFs, while Brca2 depletion had a significant impact in displaying ALT features. Taken together, we suggest that the absence of Brca2 in telomerase-null background resulted in profound replication stress at telomeres, then the resection of stalled replication forks by Mre11, leading to the instigation of a specific recombination mechanism, other than HDR, and ALT induction.

Next, we asked if Rad52 is involved. In yeast, Rad59, a paralog of Rad52, is essential in type II survivor pathway in telomerase-deficient strains [2]. Moreover, Rad52 is involved in Break-induced replication (BIR) that has been suggested for a second molecular mechanism of ALT [4,36]. APB formation in double-null MEFs was moderately decreased when Rad52 was depleted by shRNA (Fig. 4C, +4-OHT + *shRad52*). When the inhibitor for Rad52, AICAR [37], was employed, the effect of compromising APB formation was recapitulated (Fig. 4D). Taken together, these results suggest that Mre11 and Rad52 are involved in the induction of Brca2-deficient ALT.

We were puzzled with the data at first because Rad51 has been implicated in the replication fork protection from Mre11 [9]. Rad51 paralogs have been implicated in the maintenance of replication forks

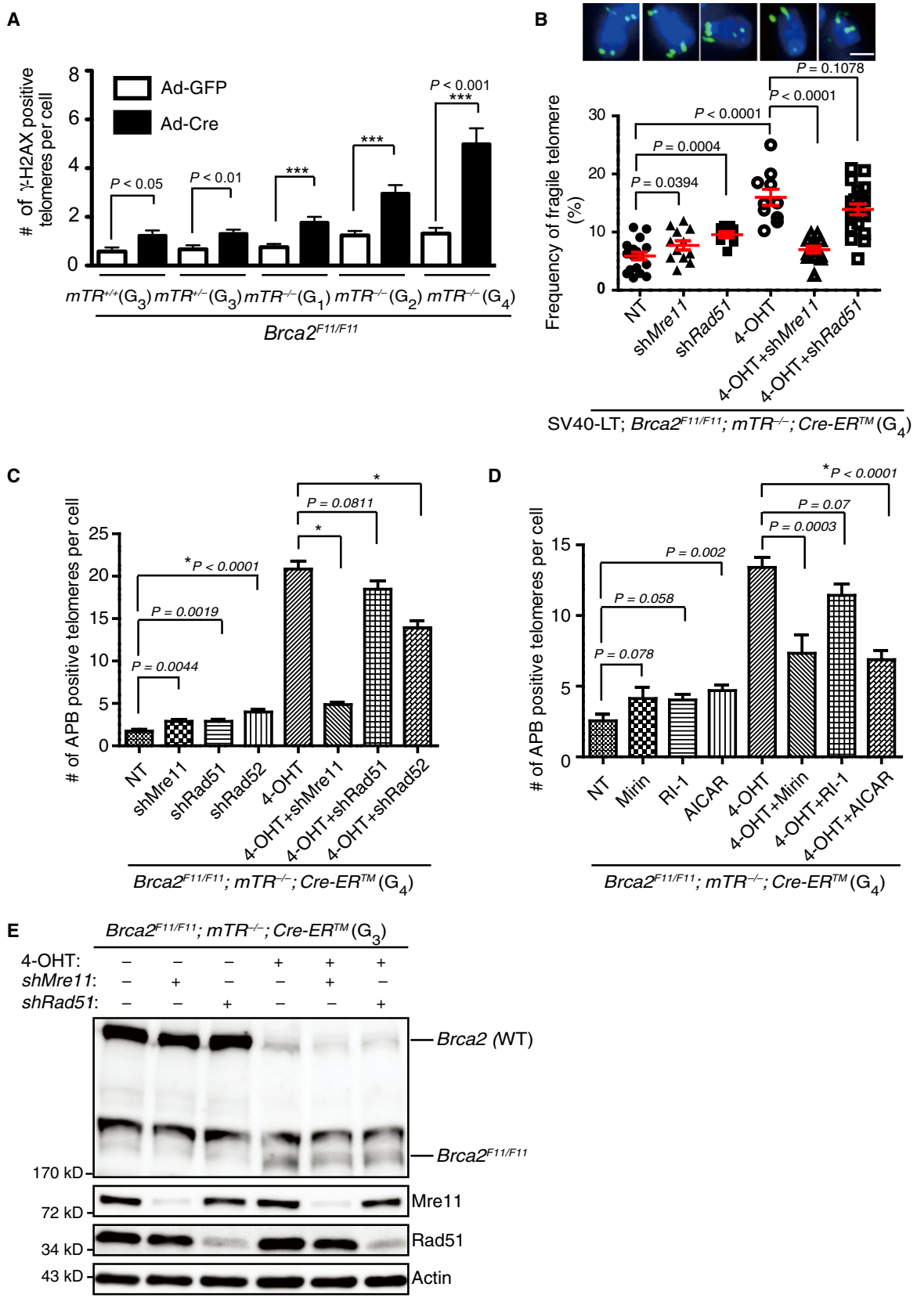
A
# of γ-H2AX positive telomeres per cell
Ad-GFP
Ad-Cre
P < 0.05
P < 0.01
***
***
P < 0.001
***
mTR+/+(G3) mTR+/−(G3) mTR−/−(G1) mTR−/−(G2) mTR−/−(G4)
Brca2F11/F11
B
P = 0.1078
P < 0.0001
P < 0.0001
P = 0.0004
P = 0.0394
Frequency of fragile telomere (%)
NT
shMre11
shRad51
4-OHT
4-OHT+shMre11
4-OHT+shRad51
SV40-LT; Brca2F11/F11; mTR−/−; Cre-ERTM (G4)
C
# of APB positive telomeres per cell
*P < 0.0001
P = 0.0811
*
*
P = 0.0019
P = 0.0044
NT
shMre11
shRad51
shRad52
4-OHT
4-OHT+shMre11
4-OHT+shRad51
4-OHT+shRad52
Brca2F11/F11; mTR−/−; Cre-ERTM (G4)
D
*P < 0.0001
P = 0.07
P = 0.0003
P = 0.002
P = 0.058
P = 0.078
# of APB positive telomeres per cell
NT
Mirin
RI-1
AICAR
4-OHT
4-OHT+Mirin
4-OHT+RI-1
4-OHT+AICAR
Brca2F11/F11; mTR−/−; Cre-ERTM (G4)
E
Brca2F11/F11; mTR−/−; Cre-ERTM (G3)
4-OHT:
shMre11:
shRad51:
Brca2 (WT)
Brca2F11/F11
170 kD
72 kD
34 kD
43 kD
Mre11
Rad51
Actin

Fig. 4. APB formation after Brca2 abrogation requires Mre11 and Rad52. (A) Conditional depletion of *Brca2* allele ($Brca2^{F11/F11}$) exacerbates telomeric DNA damage in *terc* knockout ($mTR^{-/-}$) MEFs with increase in mice generations. Bar graph represents the average number of meta-TIFs (telomere damage-induced foci in metaphase chromosomes) per cell from the MEFs. G1-G4 are the number of generations of mouse breeding with $Brca2^{F11/F11}$. MEFs of third generation $mTR^{+/+}$ and $mTR^{+/-}$ in the background of $Brca2^{F11/F11}$ mice were used for control. Metaphase chromosome spreads of indicated MEFs were subjected to γ-H2AX immunostaining, 5 days post *Ad-Cre* (black bar) or *Ad-GFP* (white bar) infection. (B) Absence of Brca2 in G4 of telomerase-deficient MEFs exhibit telomere fragility. Experiments were performed in SV40LT; $Brca2^{F11/F11}$; $mTR^{-/-}$; $Cre\text{-}ER^{TM}$ MEFs (G4). Representative images of T-FISH are shown on top. Bars, percentage of fragile telomeres. Number of metaphase chromosomes analysed: NT (control), $n = 848$; sh*Mre11*, $n = 540$; sh*Rad51*, $n = 433$; 4-OHT, $n = 467$; 4-OHT + sh*Mre11*, $n = 566$; 4-OHT + sh*Rad51*, $n = 1033$. Three independent experiments were performed (mean ± SEM). Red lines mark the average score. Scale bar, 5 μm. (C, D) Number of cells with APB. Experiments were performed in G4 MEFs of $Brca2^{F11/F11}$; $mTR^{-/-}$; $Cre\text{-}ER^{TM}$. (C) Treatment of 4-OHT creates *Brca2* mutant allele. Small hairpin RNA (*shRNA*) was employed to deplete Rad51, Rad52, Mre11, respectively, with or without Brca2 abrogation (E). Number of cells analysed: NT (control), $n = 117$; sh*Mre11*, $n = 284$; sh*Rad51*, $n = 191$; sh*Rad52*, $n = 278$; 4-OHT, $n = 336$; 4-OHT + sh*Mre11*, $n = 252$; 4-OHT + sh*Rad51*, $n = 268$; 4-OHT + sh*Rad52*, $n = 196$. Results are from three independent experiments. (D) Inhibitors targeting Mre11 (25 μM Mirin), Rad51 (20 μM RI-1), and Rad52 (20 μM AICAR), respectively, were treated with or without *Brca2*. Number of cells analysed: NT (control), $n = 38$; Mirin, $n = 108$; RI-1, $n = 135$; AICAR, $n = 102$; 4-OHT, $n = 185$; 4-OHT + Mirin, $n = 39$; 4-OHT + RI-1, $n = 119$; 4-OHT + AICAR, $n = 104$. Results are from two independent experiments. All *P* values (A–D) were obtained with the Student's *t*-test (mean ± SEM). (E) Western blot analysis; the deletion and creation of $Brca2^{F11}$ allele after tamoxifen treatment; knock-down of Mre11 after *shRNA* transfection; knock-down of Rad51 after *shRNA* transfection.

and mediate replication restart [38]. Rad51 paralogs remodel Rad51 filaments and stimulate HR [39], working together with BRCA2 and Rad51 in HR [39,40]. Furthermore, Rad51D can function at telomeres [41]. Therefore, we asked whether Rad51 paralogs are involved in ALT induction after Brca2 depletion.

Rad51C, Rad51D, Xrcc2 and Xrcc3 were depleted with shRNA in fourth telomerase-null MEFs and analysed for the telomere length, fragility and APB formation. Like Rad51 depletion, none of the tested Rad51 paralog displayed marked impact on telomere length (Fig. 5A), fragility (Fig. 5B), and APB formation (Fig. 5C). There was a slight elevation of telomere fragility after the depletion of Rad51C and Xrcc3, respectively (Fig. 5B), but the effect was not comparable to Brca2 depletion alone (Fig. 5B, +4-OHT), at least at the telomeres. Co-depletion of Rad51 and Rad51D in telomerase-null background also did not show any marked difference, suggesting that Rad51 and Rad51D are both not required.

BRCA2 depletion exhibited marked increase in telomere elongation in fourth generation of telomerase-deficient MEFs (Fig. 5A, +4-OHT). Telomeric fragility (Fig. 5B, +4-OHT) and number of APB (Fig. 5C, +4-OHT) were markedly increased as well. Notably, co-depletion of Rad51 and Rad51 paralogs with Brca2 did not alter telomere length, fragility and APB formation, respectively, compared to the effect of Brca2 depletion alone (Fig. 5). These results indicate that the ALT induction after Brca2 depletion is independent of Rad51 and Rad51 paralogs, indicating that HR is not involved.

Break-induced replication is responsible for Brca2 deficiency-induced ALT

Telomeric sister chromatid exchange (T-SCE) is frequently detected in ALT cells [42]. We and others have observed that Brca2-deficient primary cells exhibit a moderate increase in T-SCE [11,43,44]. When we assessed the degree and type of T-SCE in the third and fourth generation (G3, G4) MEFs, we observed a profound increase in T-SCE with an increase in days after Brca2 abrogation in double-null cells (Fig. 6A–C).

As double-null MEFs grew poorly in general, we immortalized the cells by introducing SV40 LT. These immortalized MEFs (Fig. 2A) were subjected to telomere CO-FISH (Chromosome Orientation-FISH) [11], and the pattern was analysed and compared to wild-type ($mTR^{+/+}$; −4-OHT). In CO-FISH assay, co-existence of leading and lagging strand signals is the indication of telomere recombination (Fig. 6A, II & III). Telomeric sister chromatid exchange taking place in unequal pattern (Fig. 6A, II, unequal T-SCE) increased from 13% at day 7 to ~ 21% at day 16 post tamoxifen treatment, whereas equal T-SCEs were barely detected (Fig. 6D). Unequal T-SCE is a sign of conservative DNA synthesis (Fig. 6D, illustrated on top), whereas the equal one is the product of semi-conservative synthesis of telomeres [5,36].

Break-induced replication (BIR) is a recombination-dependent process reinitiating DNA synthesis when one end of chromosome shares homology with the template DNA, thus leading to conservative DNA

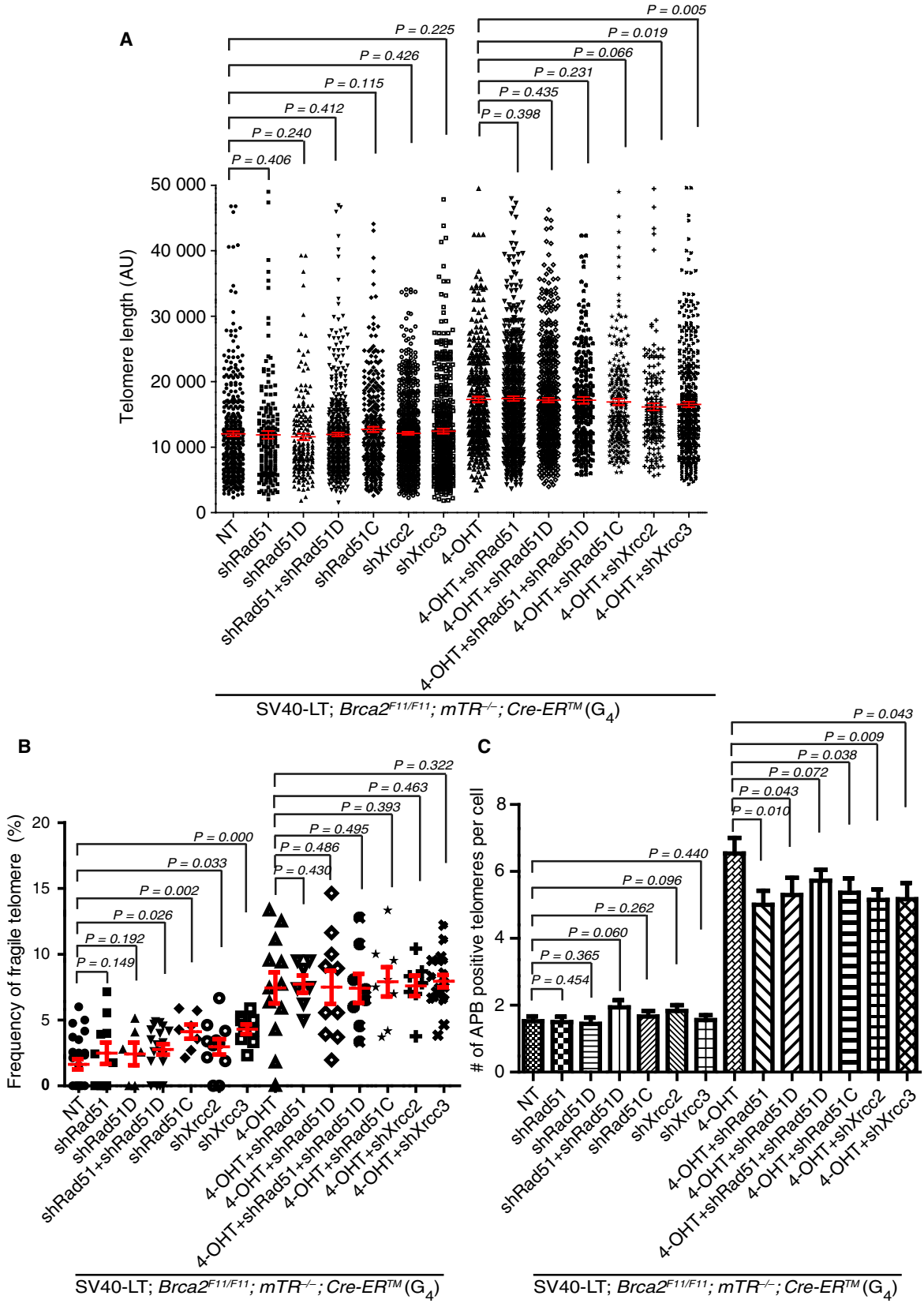
A
Telomere length (AU)
50 000
40 000
30 000
20 000
10 000
0
P = 0.225
P = 0.426
P = 0.115
P = 0.412
P = 0.240
P = 0.406
P = 0.005
P = 0.019
P = 0.066
P = 0.231
P = 0.435
P = 0.398
NT
shRad51
shRad51D
shRad51+shRad51D
shRad51C
shXrcc2
shXrcc3
4-OHT
4-OHT+shRad51
4-OHT+shRad51D
4-OHT+shRad51+shRad51D
4-OHT+shRad51C
4-OHT+shXrcc2
4-OHT+shXrcc3
SV40-LT; Brca2F11/F11; mTR−/−; Cre-ERTM (G4)
B
Frequency of fragile telomere (%)
20
15
10
5
0
P = 0.000
P = 0.033
P = 0.002
P = 0.026
P = 0.192
P = 0.149
P = 0.322
P = 0.463
P = 0.393
P = 0.495
P = 0.486
P = 0.430
SV40-LT; Brca2F11/F11; mTR−/−; Cre-ERTM (G4)
C
# of APB positive telomeres per cell
8
6
4
2
0
P = 0.440
P = 0.096
P = 0.262
P = 0.060
P = 0.365
P = 0.454
P = 0.043
P = 0.009
P = 0.038
P = 0.072
P = 0.043
P = 0.010
SV40-LT; Brca2F11/F11; mTR−/−; Cre-ERTM (G4)

Fig. 5. The induction of ALT after Brca2 abrogation is independent of Rad51 and its paralogs. (A–C) Experiments were performed in SV40LT; *Brca2*$^{F11/F11}$; *mTR*$^{-/-}$; *Cre-ER*^{TM} MEFs (G4). (A) Telomere lengths measured by T-FISH in 4th generations with (−) or without (+) 4-OHT. *Y*-axis, telomere lengths are shown as arbitrary units of fluorescence intensity from T-FISH. (B) Fragile telomeres assessed by Telomere-FISH. Number of metaphase chromosomes analysed: NT (control), $n = 993$; sh*Rad51*, $n = 335$; sh*Rad51D*, $n = 213$; sh*Rad51* + sh*Rad51D*, $n = 1062$; sh*Rad51C*, $n = 331$; sh*Xrcc2*, $n = 546$; sh*Xrcc3*, $n = 478$; 4-OHT, $n = 451$; 4-OHT + sh*Rad51*, $n = 227$; 4-OHT + sh*Rad51D*, $n = 416$; 4-OHT + sh*Rad51* + sh*Rad51D*, $n = 415$; 4-OHT + sh*Rad51C*, $n = 324$; 4-OHT + sh*Xrcc2*, $n = 346$; 4-OHT + sh*Xrcc3*, $n = 911$. (C) Number of APB-positive cells. Number of cells analysed: NT (control), $n = 59$; sh*Rad51*, $n = 70$; sh*Rad51D*, $n = 54$; sh*Rad51* + sh*Rad51D*, $n = 64$; sh*Rad51C*, $n = 60$; sh*Xrcc2*, $n = 52$; sh*Xrcc3*, $n = 70$; 4-OHT, $n = 69$; 4-OHT + sh*Rad51*, $n = 51$; 4-OHT + sh*Rad51D*, $n = 44$; 4-OHT + sh*Rad51* + sh*Rad51D*, $n = 91$; 4-OHT + sh*Rad51C*, $n = 52$; 4-OHT + sh*Xrcc2*, $n = 61$; 4-OHT + sh*Xrcc3*, $n = 29$.

synthesis. Therefore, the result from telomere CO-FISH led us to think that BIR may be responsible for the ALT induction after Brca2 abrogation. That BIR utilizes Rad52 after replication stress [45,46] supports this notion.

The induction of BIR can be corroborated by assessing the mitotic DNA synthesis, MiDAS [46], which is a conservative DNA synthesis that can take place in prophase due to incomplete DNA replication. A recent study showed that replication stress in a subset of ALT cells manifest a spontaneous mitotic DNA synthesis (MiDAS) at telomeres [36].

We asked if Brca2 abrogation led to mitotic telomere synthesis. The result showed that ~ 5% of telomeres in nearly all of double-null cells exhibited telomeric MiDAS, but none in telomerase deficiency alone (Fig. 6E). Mitotic DNA synthesis was observed in nontelomere chromosomes as well after Brca2 abrogation (Fig. 6E). However, it was detected only in cells that harboured telomeric MiDAS. Frequently, chromosomal breakage coincided with mitotic DNA synthesis (Fig. 6E), indicating that Brca2 deficiency indeed resulted in the break then subsequent BIR. While we were working on this question, a couple of papers showed that genic replication stress induced by the absence of Brca2 led to MiDAS [47,48], in agreement with our results. Approximately 2% of the whole genome, depending on how they are calculated, are transcribed. And according to comparative genomics, 8–15% of the genome is biologically functional. Therefore, the triggering of BIR at telomeres has a more profound impact in cell fate. It should be emphasized that the results shown here are not only consistent with recent publications but also extends our knowledge on the molecular basis of dysfunctional Brca2-associated tumourigenesis: Brca2 deficiency can lead to BIR-associated ALT induction. Analysing the telomere sequences by deep sequencing revealed a significant elevation of indels in double-null MEFs, further supporting that BIR is indeed induced (Fig. 6F).

Discussion

We have provided here compelling lines of evidence that the abrogation of Brca2 can induce ALT through reinforcement of BIR. When we first asked if Brca2 is a suppressor of ALT, the hypothesis was challenged by the fact that Brca2 is involved in the homology-directed repair, which was suggested as the underlying mechanism for ALT [3]. However, evidence from worms and fungus suggested that abrogation of *Brca2* orthologs can result in ALT-like phenotypes. These phenomena are consistent with the type II survivors of the telomerase-deficient yeast strain, which is devoid of Rad51 but requires Rad59, a homolog of Rad52 to maintain telomeres [2]. We have shown here that in dysfunctional telomerase mice, Brca2 deficiency instigates the pathway choice that resembles type II yeast survivor pathway.

The abrogation of Brca2 induced ALT, but many times we faced troubles in maintaining double-null cells, suggesting that an additional mutation in *p53* or checkpoint loss, indicated by SV40 LT introduction, may be required to maintain Brca2-deficient ALT cancers. Taken together, we postulate the following stepwise induction of Brca2 deficiency-associated ALT in mice and human. First, the abrogation of Brca2 will overcome senescence in cells that failed to express telomerase. In this stage, Brca2 deficiency will provoke telomere replication stress in S phase. As Brca2 is absent and HDR impaired, stalled forks are resected by the nuclease Mre11 with incomplete replication, leaving gaps between telomere repeats. If the cells continue to progress into the proliferation cycle, these gaps can be filled by the conservative DNA synthesis in prophase, using the single strand telomeres accumulated from the resection of stalled forks as primers; the break-induced replication (BIR) is induced. However, these Brca2-deficient telomerase-null cells grow poorly, but with higher mutation rate. When cells obtain mutation in *p53* or checkpoint loss will support the growth of Brca2-deficient ALT cells, leading to

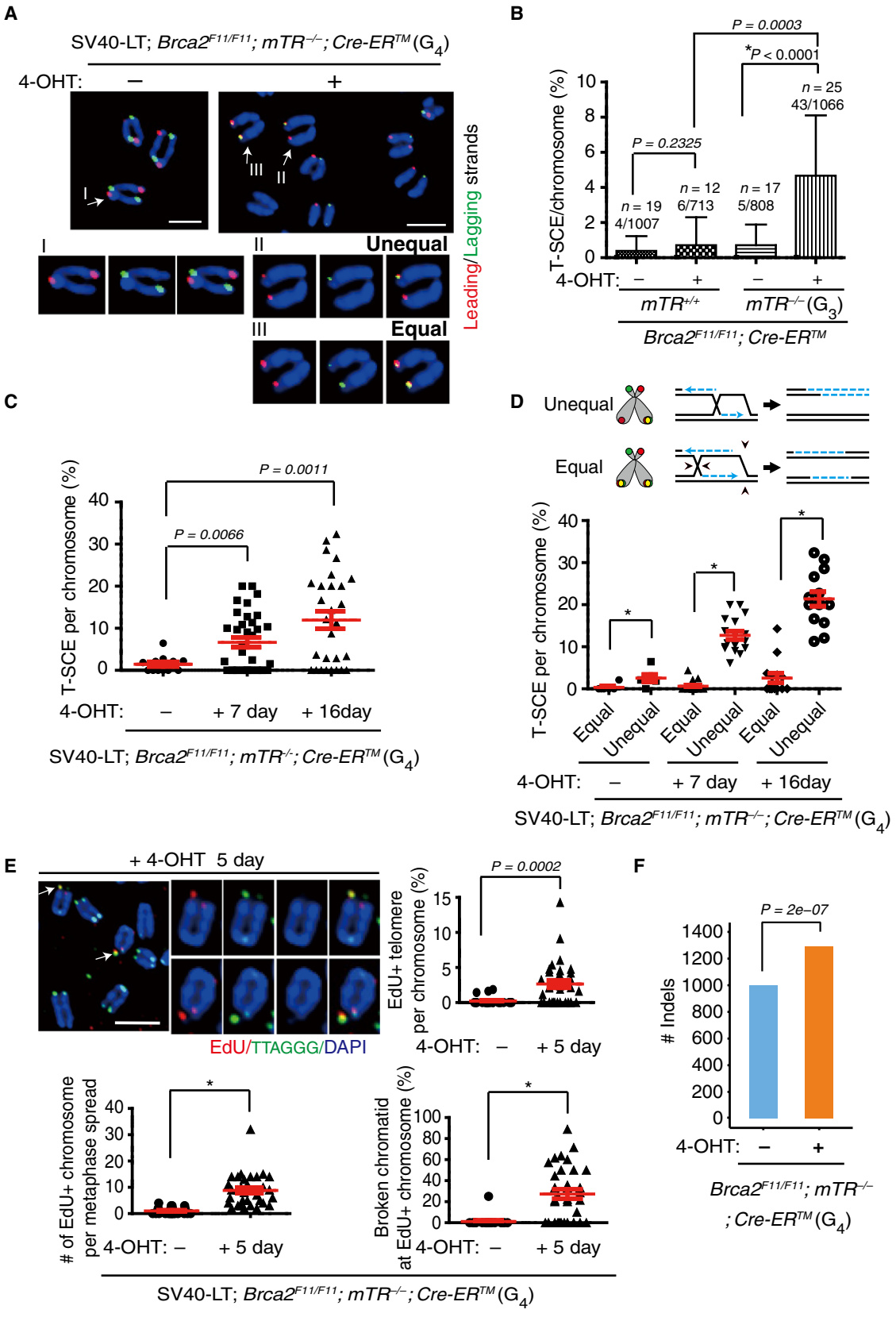
A
SV40-LT; Brca2F11/F11; mTR−/−; Cre-ERTM (G4)
4-OHT: – +
I
II
III
Unequal
Equal
Leading/Lagging strands
B
P = 0.0003
*P < 0.0001
P = 0.2325
n = 19 4/1007
n = 12 6/713
n = 17 5/808
n = 25 43/1066
T-SCE/chromosome (%)
4-OHT: – + – +
mTR+/+
mTR−/− (G3)
Brca2F11/F11; Cre-ERTM
C
P = 0.0011
P = 0.0066
T-SCE per chromosome (%)
4-OHT: – + 7 day + 16day
SV40-LT; Brca2F11/F11; mTR−/−; Cre-ERTM (G4)
D
Unequal
Equal
T-SCE per chromosome (%)
Equal Unequal Equal Unequal Equal Unequal
4-OHT: – + 7 day + 16day
SV40-LT; Brca2F11/F11; mTR−/−; Cre-ERTM (G4)
E
+ 4-OHT 5 day
EdU/TTAGGG/DAPI
P = 0.0002
EdU+ telomere per chromosome (%)
4-OHT: – + 5 day
# of EdU+ chromosome per metaphase spread
4-OHT: – + 5 day
Broken chromatid at EdU+ chromosome (%)
4-OHT: – + 5 day
SV40-LT; Brca2F11/F11; mTR−/−; Cre-ERTM (G4)
F
P = 2e–07
# Indels
4-OHT: – +
Brca2F11/F11; mTR−/− ; Cre-ERTM (G4)

Fig. 6. Brca2-deficient ALT involves conservative telomere synthesis. (A–D) Telomeric sister chromatid exchange (T-SCE) was assessed by chromosome orientation (CO)-FISH [11]. Leading and lagging strand probes localize in a diagonal orientation without T-SCE (I). The non-diagonal orientation of the leading (Red) and lagging strands (Green) represents T-SCE (arrow in II & III). Representative image of unequal T-SCE (II) and equal T-SCE (III) in Brca2-deficient telomerase-null MEFs are shown in inset. Scale bar, 5 μm. (B) The frequency of T-SCEs in bar graphs: *x*/*y*, Total number of T-SCEs/number of chromosome ends analysed; n, number of cells. (C–E) T-SCE (C, D) and MiDAS assay (E) were performed in MEFs immortalized with the transduction of SV40 LT. The effect of Brca2 abrogation in time (days after 4-OHT treatment) are compared. (D) T-SCE on single chromatid (unequal) or both chromatid end (equal) are scored. The process of DNA synthesis in equal (semi-conservative synthesis) versus unequal (conservative) T-SCE is illustrated on top. (E) The frequency of telomeric MiDAS: EdU-positive telomeres per metaphase spread were scored in the top right. Non-telomeric MiDAS were scored and shown (Bottom left). Broken chromosomes with chromosomal MiDAS were scored (Bottom right) after 4-OHT treatment for 5 days. Data are from two independent experiments (mean ± SEM). Representative image of telomeric MiDAS is shown on the top left. Scale bar, 5 μm. (A–E) Data are from two independent experiments. (F) Number of indels from telomeric sequences. *P*-value was calculated by Fisher's exact test.

neoplastic transformation (Fig. 7). We do not rule out the possibility that MUS81 nuclease might play a role in this pathway, as MUS81 is required for compensatory DNA synthesis during mitosis when Brca2 is absent [48].

Unexpectedly, the depletion of Rad51, and its paralogs as well, did not result in ALT features, unlike abrogation of Brca2 (Figs 4 and 5). This result suggests that the role of Brca2 abrogation in keeping the telomere homeostasis is independent from Rad51 and Rad51 paralogs. Rad51 and Rad51 paralogs have been implicated in the maintenance of stalled replication forks. It was expected that telomere replication stress would be increased when Rad51 or Rad51 paralogs are depleted. However, the effect was marginal, compared to the effect of Brca2 depletion alone. Therefore, it is possible that the role of Brca2 in telomere homeostasis is more than regulating HDR through Rad51 and Rad51 paralogs. Brca2 may have as-yet-unidentified association with telomere structure and protect from Mre11-mediated degradation of stalled replication forks. It would be interesting to explore if telomere-specific G-quadruplex is associated with Brca2 function.

There were indications that Brca2 depletion might induce BIR and ALT using established ALT cancer cell lines [36]. However, the process of ALT induction by the loss of Brca2 from primary cells and mice were not shown. We have shown with mouse models and the primary MEFs and organoids derived from them that Brca2 abrogation indeed is associated with the induction of ALT.

In telomerase-deficient context, telomeres shorten with proliferation then senesce. In cells that have overcome senescence from the critical shortening of telomeres, the status of Brca2 will be critical in the pathway choice associated with telomere maintenance: HDR or BIR, like type I or type II in yeast telomerase mutant survivors. Taking these pieces of information into account, assessing ALT phenotypes may be useful when targeting Brca2-mutated cancers. For example, targeting Mre11 or Rad52 may be effective to Brca2-deficient ALT cancers. It will be interesting to see if inhibitors of BIR are effective to Brca2-dysfunctional tumours that acquired resistance to poly (ADP-ribose) polymerase (PARP) inhibitors [49].

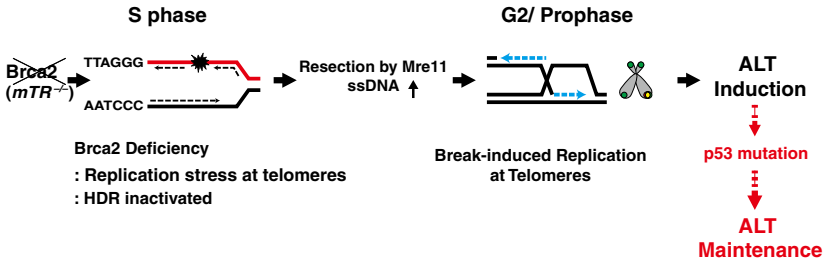

Fig. 7. Model for how Brca2 abrogation engages with ALT through the induction of BIR. Step-wise induction of Brca2-deficient ALT. In the absence of telomerase RNA, *Terc*, abrogation of Brca2 results in replication stress. Stalled replication forks are resected by Mre11, accumulating single-stranded telomeric DNA. As Brca2 is abrogated, HDR is impaired. If the cells are allowed to progress to the next cell cycle, these single-stranded telomeric DNAs trigger telomere synthesis in a conservative manner (telomeric MiDAS, BIR) in the following G2 and prophase.

Materials and methods

Animal care

Brca2^{F11} mice were from A. Berns [18] (NCI, the Netherlands). *Terc*- heterozygous knockout [50] (B6.Cg-*Terc*^{tm1Rdp}/J: also named mTR$^{+/-}$) and *Cre-ER*^{TM} transgenic [17] [B6.Cg-Tg(CAG-cre/Esr1*)5Amc/J] mice were purchased from the Jackson Laboratory. Mice were housed in a specific-pathogen free facility, and all mouse experiments were approved by the Institutional Animal Care and Use of Committee (IACUC) of Seoul National University (SNU-130219-4-9). We strictly followed the Seoul National University guidelines, politics, and regulations for the Care and Use of Laboratory Animals.

Mouse breeding, generation of MEFs, cell culture and adenoviral infection

First-generation *mTR*$^{-/-}$ MEFs were generated by the intercross of *Brca2*$^{F11/F11}$; *mTR*$^{+/-}$ mice. Second to fourth generation mice were generated by the intercrosses of former generation *Brca2*$^{F11/F11}$; *mTR*$^{-/-}$ mice. MEFs were isolated from E13.5 embryos. To delete *Brca2* allele, MEFs were infected with Cre-expressing adenovirus (Ad-Cre) at a multiplicity of 100 as previously described [11]. In the presence of *Cre-ER*^{TM}, 200 nM or 1 μM of 4-hydroxytamoxifen (4-OHT) was applied to delete *Brca2* exon 11.

Antibodies

Antibody to mouse anti-Brca2 protein was described [11]. The following antibodies were purchased: anti-Rad51 (H-92; Santa Cruz Biotechnology, Santa Cruz, CA, USA), anti-Mre11 (4895S; Cell Signaling Technology, Danvers, MA, USA), anti-phospho-Histone H2AX (Ser139) (clone JBW301, 05-636; EMD Millipore, Billerica, MA, USA), anti-PML (MAB3738; EMD Millipore), anti-actin (AC-15; Santa Cruz Biotechnology) and anti-SV40 large T antigen (SC-147; Santa Cruz Biotechnology).

Lentiviral shRNA constructs, retroviral vector, production and infection

Hairpin RNA was generated by subcloning the annealed oligonucleotides into the pLentiLox 3.7 (pLL 3.7) lentiviral vector. Oligonucleotide sequences are as follows:

shRad51 sense, 5′-TGGGAATTAGTGAAGCCAAATTCAAGAGATTTGGCTTCACTAATTCCCTTTTTTC-3′, antisense, 5′-TCGAGAAAAAAGGGAATTAGTGAAGCCAAATCTCTTGAATTTGG-CTTCACTAATTCCCA-3′; shMre11: sense, 5′-TACAGGAGAAGAGATCAACTTTCAAGA-GAAGTTGATCTCTTCTCCTGTTTTTTTC-3′, antisense, 5′-TCGAGAAAAAAACAGGA-GAAGAGATCAACTTCTCTTGAAAGTTGATCTCTTCTCCTGTA-3′. shTrp53 sense, 5′-TGTACATGTGTAATAGCTCCTTCAAGAGAGGAGCTATTACACATGTACTTTTTTC-3′, antisense, 5′-TCGAGAAAAAAGTACATGTGTAATAGCTCCTCTCTTGAAGGAGCTATTACACATGTACA-3′. shXrcc3 sense, 5′-TGACGGTTAGTCTGTCAGTATTCAAGAGATACTGACAGACTAACCGTCTTTTTTC-3′, antisense, 5′-TCGAGAAAAAAGACGGTTAGTCTGTCAGTATCTCTTGAATACTGACAGACTAACCGTCA-3′.

Lentiviral vector for *shRad52*, *shRad51C*, *shRad51D* and *shXrcc2* were purchased from Sigma Mission (Sigma-Aldrich Co., St Louis, MO, USA).

shRad52 (TRCN0000233363): CCGGTTGAAGGTCATCGGGTAATTACTCGAGTAATTACCCGATGACCTTCAATTTTTG. *shRad51C* (TRCN0000071259): CCGGCCCTTCGTACTCGATTACTAACTCGAGTTAGTAATCGAGTACGAAGGGTTTTTG *shRad51D* (TRCN0000324997): CCGGGATGATAGACATTGGGACATTCTCGAGAATGTCCCAATGTCTATCATCTTTTTG *shXrcc2* (TRCN0000294883): CCGGGCACTAAGGCAAGTCTTTAAACTCGAGTTTAAAGACTTGCCTTAGTGCTTTTTG

Lentiviral packaging plasmid psPAX2 (#12260) and envelope plasmid pMD2.G (#12259) were obtained from Addgene company (Cambridge, MA, USA). To generate lentiviral particles, Lenti-shRNA constructs were transfected into 293FT cells using lipofectamine 2000 (Invitrogen, Carlsbad, CA, USA). Lentiviral supernatant was collected and concentrated using a Lenti-X concentrator (631232; Clontech, Mountain View, CA, USA). Lentiviral infection of target cells was performed in the presence of 4 μg·mL^{-1} polybrene (Hexadimethrine bromide, H9268; Sigma-Aldrich). Efficiency of lentiviral infection was tested by observing GFP signals 2 days after infection.

C-circle assay

Genomic DNA was prepared and digested with *Mbo*I/*Alu*I. The CC assay was performed as described [26] with slight modifications. Genomic DNA was incubated with equal amount of phi29 DNA polymerase reaction. Results from hybridization with telomere probes were obtained by exposure to FLA 7000, and signal intensity was quantified using MULTI GAUGE V3.0 software (Fujifilm, Tokyo, Japan).

Microscopy and time-lapse imaging

Fluorescence microscopy images were acquired using a CoolSNAP HQ^2 cooled CCD camera on a DeltaVision Spectris Restoration microscope built around an Olympus IX70 stand with a 100 × NA 1.4 or 60 × NA 1.42 numerical aperture lens (GE Healthcare Life Sciences, Chicago, IL, USA). For live cell imaging of telomeres, MEFs were cultured in the absence or presence of 200 nM 4-OHT for 24 h and changed into fresh DMEM supplemented with

16% FBS. After 2 days, MEFs were transfected with *EGFP-TRF1* or *DsRed-PML4* plasmid and seeded onto a glass-bottom dish and analysed after 1 day. The images were acquired using a 40 × NA 1.30 objective on a microscope in a CO_2 chamber at 37 °C as previous described [28,51,52]. Images were deconvoluted using the iterative algorithm in SOFTWORX software (GE Healthcare Life Sciences).

Telomere-fluorescence *in situ* hybridization, quantitative-FISH and chromosome orientation-FISH

Metaphase chromosome spreads and telomere-fluorescence *in situ* hybridization (T-FISH) were performed as previously described [53]. Briefly, metaphase spreads on Fisherbrand™ Superfrost Plus Microscope Slides (FIS#12-550-15; Fisher Scientific, Hampton, NH, USA) were washed in 1 × PBS and dehydrated in 70%, 90% and 100% ethanol. After air drying, metaphase spreads were hybridized with Tel-Cy3 PNA probe (F1002-5; PANAGENE, Daejeon, South Korea). For quantitative-FISH, telomere-fluorescence intensity was analysed using TFL-TELO software (Peter Lansdorp, University of British Columbia). CO-FISH was performed as previously described [11]. TelG-Cy3 (F1006-5; PANAGENE) and TelC-FAM (F1001-5; PANAGENE) telomeric PNA probes were used for CO-FISH analysis.

Meta-TIF assay

The meta-TIF assay was carried out as previously described [54]. Briefly, cells were cytocentrifuged onto Superfrost Plus Microscope Slides at 450 ***g*** for 10 min in a Shandon Cytospin 4 (Thermo Scientific, Waltham, MA, USA) and then fixed immediately with 4% paraformaldehyde in 1× PBS. Slides were treated with γ-H2AX antibody at 4 °C overnight and with secondary antibody for 1 h at RT. Hybridization was performed with TelC-Cy3 PNA probe in hybridization solution [70% formamide, 10 mM Tris (pH 7.5), 0.25% blocking reagent (Roche, Basel, Switzerland) and 0.5% $MgCl_2$]. Colocalization between γ-H2AX foci and telomeric signals was analysed.

Telomeric MiDAS assay

The synchronization of the cells and 5-ethynyl-2′-deoxyuridine (EdU) labelling were performed as previously described [46] with slight modifications. Briefly, MEFs were synchronized in late G2 with CDK1 inhibitor RO-3306 (S7747; Selleckchem, Houston, TX, USA) for 16 h and then released into fresh medium with 50 μM EdU (NE08701, Carbosynth, Compton, Berkshire, UK). T-FISH, coupled with EdU staining, was performed.

Detection of telomeric repeat

To enrich for telomeric DNA, genomic DNA was digested with frequent-cutting restriction enzymes *Alu*I and *Mbo*I (New England Biolabs, Ipswich, MA, USA). Fragments > 10 kilobases (kb) were isolated and purified using Zymoclean™ Large Fragment DNA Recovery Kit (Zymo Research, Irvine, CA, USA). The purified DNA was used to generate a library using the Accel-NGS® 2S Plus DNA Library Kit and the Accel-NGS 2S Indexing Adapter Kit following the manufacturer instructions (Swift Biosciences, Ann Arbor, MI, USA). The resulting library was run on an Illumina MiSeq platform generating 300-base-pair (bp) indexed paired-end reads.

Telomere sequence analysis

Adaptor sequences on the high-throughput sequencing reads were trimmed by CUTADAPT (v1.4.1) [55]. The sequence read containing more than two telomeric repeat units (TTAGGG or CCCTAA) with mean quality score of 30 were selected as a putative telomere sequence. From the $Brca2^{F11/F11}$; CreER™; $mTR^{-/-}$ MEFs (G4) with or without 4-OHT, 57 928 reads or 55 150 reads were selected respectively. Telomeric non-hexamer repeat units within canonical telomeric hexamer repeat were regarded as telomeric indels. The telomeric indels were classified by their sequence.

Quantification and statistical analysis

GRAPHPAD PRISM 5 software (GraphPad Software, San Diego, CA, USA) was used for drawing all other graphs and statistical analysis. The Student's *t*-test was used for calculating *P* values unless stated otherwise. The mean ± SEM is shown when appropriate.

Acknowledgements

We thank the members of the Lee laboratory and E. Park (UNIST) for technical assistance, mouse breeding and critical discussions throughout the study. This work was supported by the Samsung Science and Technology Foundation (SSTF-BA1301-05).

Conflict of interest

The authors declare no conflict of interest.

Author contributions

HL directed the study and wrote the manuscript. M-SK designed and performed major experiments. JJL, JM and KH carried out the molecular analysis in mice. BCK and E-HK developed and performed mouse telomere sequencing. JB and SGP analysed telomere sequences.

References

1 Cesare AJ & Reddel RR (2010) Alternative lengthening of telomeres: models, mechanisms and implications. *Nat Rev Genet* **11**, 319–330.

2 Chen Q, Ijpma A & Greider CW (2001) Two survivor pathways that allow growth in the absence of telomerase are generated by distinct telomere recombination events. *Mol Cell Biol* **21**, 1819–1827.

3 Cho NW, Dilley RL, Lampson MA & Greenberg RA (2014) Interchromosomal homology searches drive directional ALT telomere movement and synapsis. *Cell* **159**, 108–121.

4 Dilley RL, Verma P, Cho NW, Winters HD, Wondisford AR & Greenberg RA (2016) Break-induced telomere synthesis underlies alternative telomere maintenance. *Nature* **539**, 54–58.

5 Roumelioti FM, Sotiriou SK, Katsini V, Chiourea M, Halazonetis TD & Gagos S (2016) Alternative lengthening of human telomeres is a conservative DNA replication process with features of break-induced replication. *EMBO Rep* **17**, 1731–1737.

6 Lee H (2014) Cycling with BRCA2 from DNA repair to mitosis. *Exp Cell Res* **329**, 78–84.

7 Thorslund T & West SC (2007) BRCA2: a universal recombinase regulator. *Oncogene* **26**, 7720–7730.

8 Venkitaraman AR (2009) Linking the cellular functions of BRCA genes to cancer pathogenesis and treatment. *Annu Rev Pathol* **4**, 461–487.

9 Schlacher K, Christ N, Siaud N, Egashira A, Wu H & Jasin M (2011) Double-strand break repair-independent role for BRCA2 in blocking stalled replication fork degradation by MRE11. *Cell* **145**, 529–542.

10 Lomonosov M, Anand S, Sangrithi M, Davies R & Venkitaraman AR (2003) Stabilization of stalled DNA replication forks by the BRCA2 breast cancer susceptibility protein. *Genes Dev* **17**, 3017–3022.

11 Min J, Choi ES, Hwang K, Kim J, Sampath S, Venkitaraman AR & Lee H (2012) The breast cancer susceptibility gene BRCA2 is required for the maintenance of telomere homeostasis. *J Biol Chem* **287**, 5091–5101.

12 Badie S, Escandell JM, Bouwman P, Carlos AR, Thanasoula M, Gallardo MM, Suram A, Jaco I, Benitez J, Herbig U *et al.* (2010) BRCA2 acts as a RAD51 loader to facilitate telomere replication and capping. *Nat Struct Mol Biol* **17**, 1461–1469.

13 Kwon MS, Min J, Jeon HY, Hwang K, Kim C, Lee J, Joung JG, Park WY & Lee H (2016) Paradoxical delay of senescence upon depletion of BRCA2 in telomerase-deficient worms. *FEBS Open Bio* **6**, 1016–1024.

14 Yu EY, Hsu M, Holloman WK & Lue NF (2018) Contributions of recombination and repair proteins to telomere maintenance in telomerase-positive and negative *Ustilago maydis*. *Mol Microbiol* **107**, 81–93.

15 Blasco MA, Lee HW, Hande MP, Samper E, Lansdorp PM, DePinho RA & Greider CW (1997) Telomere shortening and tumor formation by mouse cells lacking telomerase RNA. *Cell* **91**, 25–34.

16 Lee HW, Blasco MA, Gottlieb GJ, Horner JW II, Greider CW & DePinho RA (1998) Essential role of mouse telomerase in highly proliferative organs. *Nature* **392**, 569–574.

17 Hayashi S & McMahon AP (2002) Efficient recombination in diverse tissues by a tamoxifen-inducible form of Cre: a tool for temporally regulated gene activation/inactivation in the mouse. *Dev Biol* **244**, 305–318.

18 Jonkers J, Meuwissen R, van der Gulden H, Peterse H, van der Valk M & Berns A (2001) Synergistic tumor suppressor activity of BRCA2 and p53 in a conditional mouse model for breast cancer. *Nat Genet* **29**, 418–425.

19 Stange DE, Koo BK, Huch M, Sibbel G, Basak O, Lyubimova A, Kujala P, Bartfeld S, Koster J, Geahlen JH *et al.* (2013) Differentiated Troy+ chief cells act as reserve stem cells to generate all lineages of the stomach epithelium. *Cell* **155**, 357–368.

20 Boj SF, Hwang CI, Baker LA, Chio II, Engle DD, Corbo V, Jager M, Ponz-Sarvise M, Tiriac H, Spector MS *et al.* (2015) Organoid models of human and mouse ductal pancreatic cancer. *Cell* **160**, 324–338.

21 Goggins M, Schutte M, Lu J, Moskaluk CA, Weinstein CL, Petersen GM, Yeo CJ, Jackson CE, Lynch HT, Hruban RH *et al.* (1996) Germline BRCA2 gene mutations in patients with apparently sporadic pancreatic carcinomas. *Cancer Res* **56**, 5360–5364.

22 Patel KJ, Yu VP, Lee H, Corcoran A, Thistlethwaite FC, Evans MJ, Colledge WH, Friedman LS, Ponder BA & Venkitaraman AR (1998) Involvement of Brca2 in DNA repair. *Mol Cell* **1**, 347–357.

23 Lee H, Trainer AH, Friedman LS, Thistlethwaite FC, Evans MJ, Ponder BA & Venkitaraman AR (1999) Mitotic checkpoint inactivation fosters transformation in cells lacking the breast cancer susceptibility gene, Brca2. *Mol Cell* **4**, 1–10.

24 Connor F, Bertwistle D, Mee PJ, Ross GM, Swift S, Grigorieva E, Tybulewicz VL & Ashworth A (1997) Tumorigenesis and a DNA repair defect in mice with a truncating Brca2 mutation. *Nat Genet* **17**, 423–430.

25 Poon SS, Martens UM, Ward RK & Lansdorp PM (1999) Telomere length measurements using digital fluorescence microscopy. *Cytometry* **36**, 267–278.

26 Henson JD, Cao Y, Huschtscha LI, Chang AC, Au AY, Pickett HA & Reddel RR (2009) DNA C-circles are specific and quantifiable markers of alternative-lengthening-of-telomeres activity. *Nat Biotechnol* **27**, 1181–1185.

27 Smogorzewska A, van Steensel B, Bianchi A, Oelmann S, Schaefer MR, Schnapp G & de Lange T (2000)

Control of human telomere length by TRF1 and TRF2. *Mol Cell Biol* **20**, 1659–1668.
28 Choi E, Park PG, Lee HO, Lee YK, Kang GH, Lee JW, Han W, Lee HC, Noh DY, Lekomtsev S *et al.* (2012) BRCA2 fine-tunes the spindle assembly checkpoint through reinforcement of BubR1 acetylation. *Dev Cell* **22**, 295–308.
29 Henson JD, Hannay JA, McCarthy SW, Royds JA, Yeager TR, Robinson RA, Wharton SB, Jellinek DA, Arbuckle SM, Yoo J *et al.* (2005) A robust assay for alternative lengthening of telomeres in tumors shows the significance of alternative lengthening of telomeres in sarcomas and astrocytomas. *Clin Cancer Res* **11**, 217–225.
30 Henson JD, Neumann AA, Yeager TR & Reddel RR (2002) Alternative lengthening of telomeres in mammalian cells. *Oncogene* **21**, 598–610.
31 Jiang WQ, Zhong ZH, Nguyen A, Henson JD, Toouli CD, Braithwaite AW & Reddel RR (2009) Induction of alternative lengthening of telomeres-associated PML bodies by p53/p21 requires HP1 proteins. *J Cell Biol* **185**, 797–810.
32 Lee YK, Park NH & Lee H (2012) Prognostic value of alternative lengthening of telomeres-associated biomarkers in uterine sarcoma and uterine carcinosarcoma. *Int J Gynecol Cancer* **22**, 434–441.
33 Jiang WQ, Zhong ZH, Henson JD, Neumann AA, Chang AC & Reddel RR (2005) Suppression of alternative lengthening of telomeres by Sp100-mediated sequestration of the MRE11/RAD50/NBS1 complex. *Mol Cell Biol* **25**, 2708–2721.
34 Dupre A, Boyer-Chatenet L, Sattler RM, Modi AP, Lee JH, Nicolette ML, Kopelovich L, Jasin M, Baer R, Paull TT *et al.* (2008) A forward chemical genetic screen reveals an inhibitor of the Mre11-Rad50-Nbs1 complex. *Nat Chem Biol* **4**, 119–125.
35 Budke B, Logan HL, Kalin JH, Zelivianskaia AS, Cameron McGuire W, Miller LL, Stark JM, Kozikowski AP, Bishop DK & Connell PP (2012) RI-1: a chemical inhibitor of RAD51 that disrupts homologous recombination in human cells. *Nucleic Acids Res* **40**, 7347–7357.
36 Min J, Wright WE & Shay JW (2017) Alternative lengthening of telomeres mediated by mitotic DNA synthesis engages break-induced replication processes. *Mol Cell Biol* **37**, e00226-17.
37 Sullivan K, Cramer-Morales K, McElroy DL, Ostrov DA, Haas K, Childers W, Hromas R & Skorski T (2016) Identification of a small molecule inhibitor of RAD52 by structure-based selection. *PLoS One* **11**, e0147230.
38 Somyajit K, Saxena S, Babu S, Mishra A & Nagaraju G (2015) Mammalian RAD51 paralogs protect nascent DNA at stalled forks and mediate replication restart. *Nucleic Acids Res* **43**, 9835–9855.
39 Taylor MRG, Spirek M, Chaurasiya KR, Ward JD, Carzaniga R, Yu X, Egelman EH, Collinson LM, Rueda D, Krejci L *et al.* (2015) Rad51 paralogs remodel pre-synaptic Rad51 filaments to stimulate homologous recombination. *Cell* **162**, 271–286.
40 Yonetani Y, Hochegger H, Sonoda E, Shinya S, Yoshikawa H, Takeda S & Yamazoe M (2005) Differential and collaborative actions of Rad51 paralog proteins in cellular response to DNA damage. *Nucleic Acids Res* **33**, 4544–4552.
41 Tarsounas M, Munoz P, Claas A, Smiraldo PG, Pittman DL, Blasco MA & West SC (2004) Telomere maintenance requires the RAD51D recombination/repair protein. *Cell* **117**, 337–347.
42 Laud PR, Multani AS, Bailey SM, Wu L, Ma J, Kingsley C, Lebel M, Pathak S, DePinho RA & Chang S (2005) Elevated telomere-telomere recombination in WRN-deficient, telomere dysfunctional cells promotes escape from senescence and engagement of the ALT pathway. *Genes Dev* **19**, 2560–2570.
43 Bodvarsdottir SK, Steinarsdottir M, Bjarnason H & Eyfjord JE (2012) Dysfunctional telomeres in human BRCA2 mutated breast tumors and cell lines. *Mutat Res* **729**, 90–99.
44 Sapir E, Gozaly-Chianea Y, Al-Wahiby S, Ravindran S, Yasaei H & Slijepcevic P (2011) Effects of BRCA2 deficiency on telomere recombination in non-ALT and ALT cells. *Genome Integr* **2**, 9.
45 Sotiriou SK, Kamileri I, Lugli N, Evangelou K, Da-Re C, Huber F, Padayachy L, Tardy S, Nicati NL, Barriot S *et al.* (2016) Mammalian RAD52 functions in break-induced replication repair of collapsed DNA replication forks. *Mol Cell* **64**, 1127–1134.
46 Bhowmick R, Minocherhomji S & Hickson ID (2016) RAD52 facilitates mitotic DNA synthesis following replication stress. *Mol Cell* **64**, 1117–1126.
47 Feng W & Jasin M (2017) BRCA2 suppresses replication stress-induced mitotic and G1 abnormalities through homologous recombination. *Nat Commun* **8**, 525.
48 Lai X, Broderick R, Bergoglio V, Zimmer J, Badie S, Niedzwiedz W, Hoffmann JS & Tarsounas M (2017) MUS81 nuclease activity is essential for replication stress tolerance and chromosome segregation in BRCA2-deficient cells. *Nat Commun* **8**, 15983.
49 Farmer H, McCabe N, Lord CJ, Tutt AN, Johnson DA, Richardson TB, Santarosa M, Dillon KJ, Hickson I, Knights C *et al.* (2005) Targeting the DNA repair defect in BRCA mutant cells as a therapeutic strategy. *Nature* **434**, 917–921.
50 Wong KK, Chang S, Weiler SR, Ganesan S, Chaudhuri J, Zhu C, Artandi SE, Rudolph KL, Gottlieb GJ, Chin L *et al.* (2000) Telomere dysfunction impairs DNA repair and enhances sensitivity to ionizing radiation. *Nat Genet* **26**, 85–88.
51 Park I, Lee HO, Choi E, Lee YK, Kwon MS, Min J, Park PG, Lee S, Kong YY, Gong G *et al.* (2013) Loss of BubR1 acetylation causes defects in spindle assembly

checkpoint signaling and promotes tumor formation. *J Cell Biol* **202**, 295–309.
52 Choi E, Choe H, Min J, Choi JY, Kim J & Lee H (2009) BubR1 acetylation at prometaphase is required for modulating APC/C activity and timing of mitosis. *EMBO J* **28**, 2077–2089.
53 Dimitrova N, Chen YC, Spector DL & de Lange T (2008) 53BP1 promotes non-homologous end joining of telomeres by increasing chromatin mobility. *Nature* **456**, 524–528.
54 Cesare AJ, Kaul Z, Cohen SB, Napier CE, Pickett HA, Neumann AA & Reddel RR (2009) Spontaneous occurrence of telomeric DNA damage response in the absence of chromosome fusions. *Nat Struct Mol Biol* **16**, 1244–1251.
55 Didion JP, Martin M & Collins FS (2017) Atropos: specific, sensitive, and speedy trimming of sequencing reads. *PeerJ* **5**, e3720.

Supporting information

Additional supporting information may be found online in the Supporting Information section at the end of the article.

Movie S1. Time-lapse video microscopy of telomere movement with TRF1-GFP. Movie for Fig. 2B, top panel. $mTR^{-/-}$ (−4-OHT).
Movie S2. Time-lapse video microscopy of telomere movement with TRF1-GFP. Movie for Fig. 2B, middle panel. TRF1-GFP. $mTR^{-/-}$ (+4-OHT).
Movie S3. Time-lapse video microscopy of telomere movement with TRF1-GFP. Movie for Fig. 2B, bottom panel. TRF1-GFP. $mTR^{-/-}$ (+4-OHT).
Movie S4. Time-lapse video microscopy of TRF1-GFP and PML4-RFP. Movie for Fig. 2F. TRF1-GFP in grey. $mTR^{-/-}$ (−4-OHT).
Movie S5. Time-lapse video microscopy of TRF1-GFP and PML4-RFP. Movie for Fig. 2F, top panel. TRF1-GFP and PML4-RFP merged. $mTR^{-/-}$ (−4-OHT).
Movie S6. Time-lapse video microscopy of TRF1-GFP and PML4-RFP. Movie for Fig. 2F, bottom panel. TRF1-GFP in grey. $mTR^{-/-}$ (+4-OHT).
Movie S7. Time-lapse video microscopy of TRF1-GFP and PML4-RFP. Movie for Fig. 2F, bottom panel. TRF1-GFP and PML4-RFP. $mTR^{-/-}$ (+4-OHT).